Coupled channel analysis of data on $\bar{p}p \to 3\pi^0$, $\eta\eta\pi^0$, and $\eta\pi^0\pi^0$ at rest, with the N/D method

D. V. Bugg
Queen Mary and Westfield College, London E1 4NS, United Kingdom

V. V. Anisovich and A. Sarantsev
Queen Mary and Westfield College, London E1 4NS, United Kingdom
and St. Petersburg Nuclear Physics Institute, Gatchina, St. Petersburg district, 188350, Russia

B. S. Zou
Queen Mary and Westfield College, London E1 4NS, United Kingdom
(Received 31 May 1994)

Details are presented from a coupled channel analysis of Crystal Barrel data on $\bar{p}p \to 3\pi^0$, $\eta\eta\pi^0$, and $\eta\pi^0\pi^0$ at rest, together with the $\pi\pi$ S-wave phase shift up to 1.2 GeV. The annihilation data are well fitted with a pure $^1S_0$ initial state using consistent parameters for resonances in all channels. The annihilation data require two $I = 0$, $J^{PC} = 0^{++}$ resonances with masses and widths M, Γ where $M_1 = 1340 \pm 40$ MeV, $\Gamma_1 = 255^{+60}_{-40}$ MeV and $M_2 = 1505 \pm 20$ MeV, $\Gamma_2 = 150 \pm 20$ MeV; the $\eta\pi^0\pi^0$ data require an $I = 1$, $J^{PC} = 0^{++}$ resonance with $M_3 = 1435 \pm 40$ MeV and $\Gamma_3 = 270 \pm 40$ MeV. The $a_0(980)$ is fitted with a Flatté form with $M = 999 \pm 5$ MeV, $g_{\eta\pi} = 221 \pm 20$ MeV, and $r = g_{KK}/g_{\eta\pi} = 1.16 \pm 0.18$. The $\eta\pi\pi$ data suggest a significantly larger width, $\Gamma = 75$ MeV, for $f_0(975)$ than earlier data. They also require an appreciable $\eta\pi$ P wave, which shows weak phase variation and is therefore probably nonresonant.

PACS number(s): 13.75.Cs, 14.40.Cs

I. INTRODUCTION

Earlier papers of the Crystal Barrel Collaboration presented data on $\bar{p}p \to 3\pi^0$ and $\eta\eta\pi^0$ at rest and amplitude analyses [1–4]. The earliest analysis [1] of $3\pi^0$ fitted the data with 60% annihilation from initial P states and 40% from $^1S_0$. This analysis required an $I = 0$, $J^{PC} = 2^{++}$ resonance called A_X at 1515 ± 10 MeV, in line with an analysis of earlier Asterix data [5]. The first publication on $\eta\eta\pi^0$ [2] claimed the existence of $I = 0$, $J^{PC} = 0^{++}$ resonances at 1430 MeV ($\Gamma = 250$ MeV) and 1560 ± 25 MeV ($\Gamma = 245 \pm 50$ MeV).

However, a later analysis [3] revealed an alternative solution for $3\pi^0$ data in which the annihilation is purely from the initial $^1S_0$ state. This was achieved using the N/D method used here. It allowed more flexibility in the numerator $N(s)$. It found $I = 0$, $J^{PC} = 0^{++}$ resonances at 1520 ± 25 MeV ($\Gamma = 148^{+20}_{-25}$ MeV) and 1365^{+20}_{-55} MeV ($\Gamma = 268 \pm 70$ MeV). The former resonance replaced the $A_X(1515)$. Some evidence remained for a small but significant 2^+ amplitude at masses above $f_2(1270)$, possibly resonating at 1555 MeV but possibly due to the $\rho\rho$ threshold anticipated at this mass. A detailed paper [4], showing a variety of fits with different formulas, revised the masses and widths of the resonances by small amounts; the masses moved to $M_1 = 1335 \pm 40$ MeV and $M_2 = 1505 \pm 20$ MeV. For consistency of notation with the Crystal Barrel paper [3], we shall continue to refer to these resonances as $f_0(1520)$ and $f_0(1365)$.

The objective of the present paper is to add to the analysis data on $\bar{p}p \to \eta\pi^0\pi^0$ at rest. These data require the $f_0(1365)$ in the $\pi\pi$ S wave. They also require an $I = 1$, $J^{PC} = 0^{++}$ resonance, reported in Ref. [6] as having $M = 1450 \pm 40$ MeV with $\Gamma = 278 \pm 40$ MeV. It is natural to interpret this resonance as the partner of $f_0(1365)$ and $K_0^*(1430)$ [7] in a $\bar{q}q$ nonet. Other conspicuous features of the $\eta\pi^0\pi^0$ data are $a_0(980)$ and $f_0(975)$ and we are able to comment on their parameters. It turns out that the fit also requires a significant but nonresonant $\eta\pi$ P wave.

Section II reviews the qualitative features of the data and gives formulas for the amplitudes. Section III gives details of the fits obtained with three variants of the formulas, so as to illustrate the possible latitude in the fits. Section IV gives conclusions.

II. INGREDIENTS

Using the N/D method, all three annihilation channels can be fitted well assuming pure $^1S_0$ annihilation. For $\eta\pi^0\pi^0$, we have tried adding P-state annihilation for $\bar{p}p \to a_2(1320)\pi$. This reaction would have an angular distribution distinctively different for initial P and S states. The fit optimizes at 3.0% for $^3P_2$ and $^3P_1$ combined. However, the reduction in χ^2 is small ($\Delta\chi^2 \simeq 20$ for 1289 points) compared with that expected for two extra parameters. Also the changes to the fit are minor. So we shall ignore possible P-state annihilation hereafter.

The $3\pi^0$ and $\eta\eta\pi^0$ data have been examined in detail in Refs. [3] and [4] and will not be discussed here in any detail. It suffices to say that the fits given there are changed very little. There are minor adjustments of

resonance parameters and coupling constants, required by addition of the $\eta\pi^0\pi^0$ data. In particular, these data require some changes to the width of $f_0(975)$.

The Dalitz plot for $\bar{p}p \to \eta\pi^0\pi^0$ data at rest is shown in Fig. 1 and we first review the salient features. There are conspicuous bands, nearly vertical and horizontal, due to $a_2(1320)$ in $\eta\pi$. In addition, there is a strikingly sharp edge at a mass $M_{\eta\pi} = 991$ MeV, the $\overline{K}K$ threshold. It is due to $a_0(980)$ interfering destructively with the $\pi\pi$ S wave. The $a_0(980)$ has decay modes of similar strength to $\eta\pi$ and $\overline{K}K$. At the $\overline{K}K$ threshold, the opening channel attenuates the $a_0 \to \eta\pi$ signal and the destructive interference gives rise to the sharp increase of the density of events above the $\overline{K}K$ threshold.

Quantitative fits require in addition to $a_0(980)$ a second $I = 1$, $J^{PC} = 0^{++}$ resonance at 1425–1450 MeV. It is not immediately evident on the Dalitz plot or on the projection to $M_{\eta\pi}$, but is revealed by systematic interferences with other strong amplitudes, notably $a_2(1320)$. We shall refer to it as $a_0(1450)$, for consistency of notation with Ref. [6], and will devote considerable attention to it in Sec. III. The solution discussed here is solution B of Ref. [6].

Next, there is a diagonal band across the Dalitz plot due to $f_0(975)$. A close look reveals an increase in intensity in the $\pi\pi$ channel above the $\overline{K}K$ threshold, for example, near the point marked A in Fig. 1. Below the $\overline{K}K$ threshold, the $f_0(975)$ is distinctly broader than earlier data have suggested. This is not due to experimental resolution, which is about ± 12 MeV near this mass. The band due to $f_0(975)$ extends down to 875 MeV, where amplitude analysis reveals a cusp in the $\pi\pi$ amplitude. The width of $f_0(975)$ will be discussed in detail in the next section.

It turns out to be rather difficult to fit the Dalitz plot around the region marked B, where the number of events is small. This region is sensitive to parameters of $f_0(975)$. The fit to this region, and at higher $M_{\eta\pi}$, requires in addition to $a_2(1320)$ and $a_0(1450)$ some further small ingredient in $\eta\pi$. It is difficult to distinguish between $J^P = 0^+$ and 2^+ in the high mass $\eta\pi$ region because of the limited phase space, but 2^+ gives a slightly better fit. The simplest way of achieving a good fit is to introduce into $\eta\pi$ a second resonance which we call $a_2'(1620)$. However, in this mass range inelasticity is expected due to $\pi\eta \to \rho\omega$ and $a_0(980)\sigma$ (where σ is a shorthand notation for the $\pi\pi$ S wave). It is therefore possible that $a_2'(1620)$ is simply mocking up the effect of the inelastic threshold, and we make no strong claim for this as a new resonance.

A. Data selection

The present analysis uses 50 000 events on $\bar{p}p \to 3\pi^0$ from Ref. [1] and 20 000 events on $\bar{p}p \to \eta\eta\pi^0$ from Ref. [2]. For $\eta\pi^0\pi^0$, there are two data sets available within the Crystal Barrel Collaboration. The earlier set, containing 108 000 events, has been reported at conferences [8]; details of the analysis procedure are given by Winter [9]. Subsequent processing of more data has yielded 280 000 events. The former data set is used in this publication, partly for historical reasons; it was available at the time when much of the fitting was being done. Second, fits to the later set reveal a poor χ^2 for edge bins: χ^2 per degree of freedom (DF) changes from 1.65 to 1.3 when all bins at the immediate edge of the Dalitz plot are dropped. This problem is not present in the earlier data set. Since edge bins play an important role in much of the physics, particularly the enhancement marked C in Fig. 1, we use the earlier data set. The statistical errors, even for 108 000 events, are overwhelmed by systematic

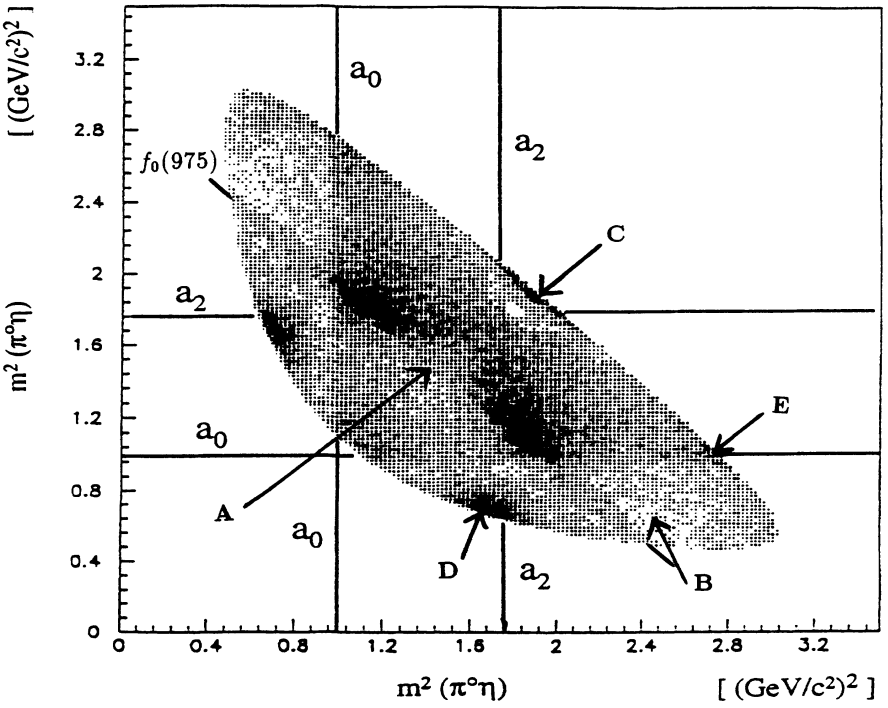

FIG. 1. The Dalitz plot for $\bar{p}p \to \eta\pi^0\pi^0$ at rest.

uncertainties depending on which algebraic forms are to be fitted to the data.

The Dalitz plot is folded about the diagonal and divided into 1289 bins. There are 29 or 31 parameters in the various forms fitted to the $\eta\pi^0\pi^0$ data, leaving 1260 or 1258 DF.

B. Formulas

The motivation behind the N/D method is discussed at length in Ref. [4] and will not be elaborated here. We repeat essential formulas, so as to define parameters given in tables of amplitudes.

We start with $\eta\pi$ amplitudes. For the $a_0(980)$ S-wave amplitude, we use the Flatté parametrization [10]

$$f_{980} = \frac{\Lambda_{980}}{s - M^2 + iM(\rho_1 g_1 + \rho_2 g_2)}, \tag{1}$$

where we take $\eta\pi$ as channel 1 and $K\overline{K}$ as channel 2; ρ are phase volumes,

$$\rho = 2q/\sqrt{s} = \frac{\sqrt{[s-(m_1+m_2)^2][s-(m_1-m_2)^2]}}{s}, \tag{2}$$

q is the momentum in the final state, and below the $K\overline{K}$ threshold we make the analytic continuation

$$\rho_2 = +i\sqrt{(4m_K^2 - s)/s}. \tag{3}$$

For $a_0(1450)$, we take

$$f_{1450} = \frac{\Lambda_{1450}}{s - M^2 + iMg\rho_{\eta\pi}}. \tag{4}$$

This resonance lies at a mass where the inelastic thresholds for $a_0(980)\sigma$ and $\rho\omega$ may be opening, and so we have also tried adding a four-particle decay width for these channels, or using it to replace $g\rho$ in the denominator of f_{1450}; formulas for these refinements are given later in Sec. III. They make a negligible difference to the fit, $\Delta\chi^2 < 5$.

Alternative K-matrix parametrizations have been tried for the $\eta\pi$ S wave, but give almost identical fits and pole positions. Since the formulas are less transparent than Breit-Wigner amplitudes, we shall not give details here.

For $a_2(1320)$ we take

$$f_{1320} = \frac{\Lambda_{1320} B_2(p) B_2(q) P_2(\cos\theta)}{s - M^2 + iM\Gamma}, \tag{5}$$

$$\Gamma = gB_2^2(q)\rho_{\eta\pi}, \tag{6}$$

where $q(s)$ is the decay momentum of the resonance in its rest frame and $p(s)$ is the production momentum in the overall center of mass. The angle θ is the decay angle of the resonance in its center of mass and is evaluated between p and q. We have also tried replacing $\rho_{\eta\pi}$ in the denominator of the Breit-Wigner amplitude by $\rho_{\rho\pi}$, corresponding to the dominant decay mode; this has a negligible effect, as does the explicit inclusion of the $K\overline{K}$ decay width of $a_2(1320)$. For the centrifugal barrier in the case of production of P- and D-wave resonances, we use the Hippel-Quigg forms (after some algebraic manipulation):

$$B_J(p) = F_J/F_J(\text{res}), \tag{7}$$

$$F_2(p) = \frac{p^2}{[p^2(p^2 + X_2) + X_2^2]^{1/2}}, \tag{8}$$

$$F_1(p) = \frac{p}{(p^2 + X_1)^{1/2}}, \tag{9}$$

and

$$X_2 = 0.356\ \text{GeV}^2, \tag{10}$$

$$X_1 = X_2/3. \tag{11}$$

The value $F_J(\text{res})$ is evaluated on resonance, i.e., at $s = M^2$. The parameter X_2 has been optimized by fitting to the shape of $a_2(1320)$ and $f_2(1270)$ in $\eta\pi^0\pi^0$ and $\pi^0\pi^0\pi^0$ data, respectively, and corresponds to a radius of interaction of 0.57 fm. We assume that the same radius of interaction can be used for other resonances. For $a_2'(1620)$ we use the same algebraic expression as for $a_2(1320)$.

A variety of forms for the $\pi\pi \to \pi\pi$ and $\pi\pi \to K\overline{K}$ S-wave amplitudes are discussed at length in papers by Zou and Bugg [11] and Anisovich *et al.* [4]. The essence of the situation is as follows. In fitting annihilation data, we have tried several quite different forms, based on a T-matrix formalism or on K matrices. Up to $M_{\pi\pi}$, all give very similar results. For the purposes of fitting $\eta\pi^0\pi^0$ data, this is almost sufficient, since phase space for $\pi\pi$ ends at 1328 MeV. For fitting $3\pi^0$ data and $\eta\eta\pi^0$, it does matter and is discussed at length by Anisovich *et al.* [4]. The problem is that annihilation data provide firm evidence for two f_0 resonance at about 1365 and 1520 MeV, but these are not resolved in the CERN-Munich data [12] on $\pi\pi \to \pi\pi$, from which the $\pi\pi$ S-wave phase shift δ_S has traditionally been deduced [13]. In the present paper, we shall describe fits based on three alternative fits to δ_S, in order to illustrate the latitude presently allowed by annihilation data.

The scattering amplitude for $\pi\pi \to \pi\pi$ and $K\overline{K}$ will be written in terms of a 2×2 K matrix:

$$T = K(I - i\rho K)^{-1}, \tag{12}$$

$$T_{11} = \frac{K_{11} - i\rho_2(K_{11}K_{22} - K_{12}^2)}{D}, \tag{13}$$

$$D = 1 - i\rho_1 K_{11} - i\rho_2 K_{22} - \rho_1\rho_2(K_{11}K_{22} - K_{12}^2), \tag{14}$$

$$\rho_1 = (1 - 4m_\pi^2/s)^{1/2}, \quad m_\pi = 134.96\ \text{MeV}, \tag{15}$$

$$\rho_2 = (1 - 4m_K^2/s)^{1/2} \text{ for } s > 4m_K^2, \quad m_K = 495.67\ \text{MeV}, \tag{16}$$

$$= +i(4m_K^2/s - 1)^{1/2} \text{ for } s < 4m_K^2. \tag{17}$$

In the first parametrization, labeled A, matrix elements K_{ij} are written

$$K_{ij} = \left(\frac{s - 2m_\pi^2}{s}\right)\left(\frac{\alpha_i\alpha_j}{s_A - s} + \frac{\beta_i\beta_j}{s_B - s} + \frac{\gamma_i\gamma_j}{s_C - s} + A_{ij} + B_{ij}s\right). \quad (18)$$

Numerical values of the parameters are given in Table I. This form has been used for most of the systematic checks on data, but has been compared with two other variants B and C given below.

In fitting annihilation data, the S-wave $\pi\pi$ amplitude is written

$$T = \frac{N(s)}{D(s)} + \frac{\Lambda_{1365}}{s - M_1^2 + iM_1\rho g_1} + \frac{\Lambda_{1520}}{s - M_2^2 + iM_2\rho g_2}. \quad (19)$$

The denominator $D(s)$ of the first term is identical to that in $\pi\pi$ elastic scattering. The numerator $N(s)$, however, has left-hand cuts which are quite different between $\pi\pi$ elastic scattering and annihilation reactions. In order to fit the annihilation data flexibly, the most general form we have adopted is

$$N_{\pi\pi}(s) = \left(\Lambda_1 + \Lambda_2 s + \frac{\Lambda_4}{s - s_0}\right)K_{11} + i\rho_2(\Lambda_3 + \Lambda_5 s)D_K, \quad (20)$$

$$D_K = K_{11}K_{22} - K_{12}^2. \quad (21)$$

Here Λ_i are complex coupling parameters. Other forms have been tried in which the determinant D_K is replaced by a variety of other expressions, e.g., K_{12}, but in practice the one given here has the virtue of rapid numerical convergence, because K_{11} and D_K happen to be nearly orthogonal functions.

In practice, five Λ parameters in Eq. (20) are too many, and convergence is poor. Therefore we have omitted Λ_4 in all work except tests. In some parametrizations described below, Λ_5 is negligible. At least three Λ parameters are always required and must be complex. With three Λ parameters, numerical convergence is rapid and stability is excellent.

Form A, Eq. (18), for the $\pi\pi$ S wave fits CERN-Munich data up to 1.8 GeV. However, it suffers from a potential difficulty. The amplitude has a broad pole at about 1500 MeV, which may be simulating unresolved $f_0(1365)$ and $f_0(1520)$ resonances. These latter resonances are added to the fit to annihilation data, Eq. (19), and so there is the danger of double counting. In particular, this makes the determination of branching ratios difficult.

Our second alternative, labeled B, is to use this formula in fitting annihilation data only up to $s = 1.2$ GeV^2. At higher energies, $f_0(1365)$ and $f_0(1520)$ are introduced plus a parabolic background,

$$\frac{N(s)}{D(s)} = \Lambda_a + \Lambda_b s + \Lambda_c s^2, \quad (22)$$

which is joined smoothly to the form A at $s = 1.2$ GeV^2. This explicitly eliminates double counting in the mass range of $f_0(1365)$ and $f_0(1520)$. It gives very similar results to A.

Our third parametrization, labeled C is

$$K_{11} = \frac{g_1(s)}{g_0(s)}, \qquad K_{22} = \frac{g_2(s)}{g_0(s)}, \quad (23)$$

$$K_{12} = K_{21} = \frac{\sqrt{g_1(s)g_2(s) - g_0(s)g_3(s)}}{g_0(s)}, \quad (24)$$

where

$$g_0(s) = (s - s_1)(s - s_2), \quad (25)$$

$$g_1(s) = \gamma_1 + \gamma_2 s, \quad (26)$$

$$g_2(s) = \gamma_3 + \gamma_4 s, \quad (27)$$

$$g_3(s) = \gamma_5 + \gamma_6 s. \quad (28)$$

This form fits the $\pi\pi \to \pi\pi$ data well up to $s = 1.2$ GeV^2. Above this mass, the additional poles due to $f_0(1365)$ and $f_0(1520)$ fit the annihilation data. Parameter values are given in Table II. For this form, the nonrelativistic centrifugal barriers F_2 and F_1 of Eqs. (8) and (9) are replaced by relativistic forms. Formulas, which are lengthy, are given in Ref. [4]. The barrier factor X_2 of Eq. (10) is set to the value $X_2 = 0.106$ GeV^2, corresponding to a radius of interaction of 1 fm. After readjustment of coupling constants, results for relativistic and nonrelativistic centrifugal barriers are almost indistinguishable.

In fitting $\eta\eta\pi$ data, we include $a_0(1450)$, taking the coupling constant from

$$\Lambda_{1450}(\eta\eta\pi) = \Lambda_{980}(\eta\eta\pi)\frac{\Lambda_{1450}(\eta\pi\pi)}{\Lambda_{980}(\eta\pi\pi)}. \quad (29)$$

However, since the $\eta\pi$ phase space in $\eta\eta\pi$ data stops at $M = 1334$ MeV, the $a_0(1450)$ has only a small (but beneficial) effect in fitting $\eta\eta\pi$ data.

Likewise, in fitting $\eta\pi\pi$ data, we use a corresponding way of including $f_0(1520)$:

$$\Lambda_{1520}(\eta\pi\pi) = \Lambda_{1365}(\eta\pi\pi)\frac{\Lambda_{1520}(3\pi^0)}{\Lambda_{1365}(3\pi^0)}. \quad (30)$$

TABLE I. K matrix parameters of Eq. (18) fitted to $3\pi^0$, $\eta\pi^0\pi^0$, and CERN-Munich phase-shift data. Units are GeV.

$s_A = 0.7389$	$\alpha_1 = 0.7469$	$\alpha_2 = 0$
$s_B = 1.4369$	$\beta_1 = 1.0287$	$\beta_2 = -0.1342$
$s_C = 3.9168$	$\gamma_1 = 1.3838$	$\gamma_2 = -2.3465$
$A_{11} = -1.1500$	$A_{12} = 1.6209$	$A_{22} = -1.0186$
$B_{11} = 0.4390$	$B_{12} = 0$	$B_{22} = 0$

TABLE II. K-matrix parameters of Eqs. (25)–(28) fitted to $3\pi^0$, $\eta\pi^0\pi^0$, and CERN-Munich phase-shift data. Units are GeV.

$s_1 = 0.0006$	$s_2 = 1.5763$
$\gamma_1 = 4.5893$	$\gamma_2 = -4.8286$
$\gamma_3 = 2.4496$	$\gamma_4 = -1.9089$
$\gamma_5 = -0.8890$	$\gamma_6 = 1.8197$

The contribution within the phase space available is small.

Having defined the equations for the amplitudes, we now discuss each contribution in turn.

C. $a_0(980)$

This is one of the key elements in the fit. It shows up strongly through the sharp edge it produces at the $K\overline{K}$ threshold; see Fig. 1. The edge in the data agrees with the mean mass of K^0K^0 and K^+K^- within 2 MeV if the mean mass is fitted in Eqs. (16) and (17).

As parameters in the Flatté form, Eq. (1), we choose to fit M, g_1, and $r = g_2/g_1$, i.e., the ratio of couplings to $K\overline{K}$ and $\eta\pi$. What emerges from the fits is that the parameters M, g_1, and r are strongly correlated. If any one of them, say, r, is moved in steps, χ^2 changes rather slowly, but M, g_1, and r move together. Table III illustrates the correlation when parameters of $a_0(980)$ are fitted freely to $\eta\pi^0\pi^0$ and $\eta\eta\pi^0$ data. This correlation should come as no surprise. A glance at Fig. 1 reveals that one cannot expect to get a good determination of mass and width for the $a_0(980)$ from $\eta\pi^0\pi^0$ data, since there is no visible peak. Nonetheless, there is great phase sensitivity in the interference of $a_0(980)$ with the $\pi\pi$ S wave, and so we are in a position to improve greatly on previous knowledge of $a_0(980)$.

In order to break this correlation, we introduce into the fit two constraints from other Crystal Barrel data on $\overline{p}p \to \omega\eta\pi^0$ at rest [14]. There the peak due to $a_0(980)$ is clearly visible and gives an excellent determination of the mass and width. The present fits are constrained with the masses at which the $a_0(980)$ cross section falls to half-height. These are at 954.9 and 1013.3 MeV, where the $a_0(980)$ cross section has been convolved with an energy resolution of ± 11 MeV. This constraint has a dramatic effect in stabilizing the fit; see Table IV. At a later stage of the discussion, we shall add $a_2'(1620)$ to the fit. This reduces the optimum value of r slightly (Table VIII). The resulting determination of $r = 1.16 \pm 0.18$ is a considerable improvement on earlier work of Lockman [15]. The error is assessed conservatively from $\Delta\chi^2 = 25$, in order to allow for possible systematic effects of different parametrizations. The pole positions are at $1014 - i41$ MeV on the second sheet and $957 - i106$ MeV on the third.

TABLE III. Correlations between parameters M, g_1, and r of $a_0(980)$ without any external constraint. Fits are made to $\eta\eta\pi^0$ and $\eta\pi^0\pi^0$ data in combination. The $a_2'(1620)$ contribution is not included in the fit at this stage. M and g_1 are in MeV.

r	χ^2	M	g_1
1.05	2472.9	1012.6	241.3
1.25	2455.7	1017.5	246.0
1.35	2449.1	1022.9	254.0
1.45	2447.2	1028.2	257.9
1.65	2448.6	1036.8	269.3
1.85	2457.7	1043.3	278.9
2.05	2467.6	1057.5	286.9

TABLE IV. As in Table III, but including a constraint on $|a_0(980)|^2$ at half-height with a $\pm 2\%$ error. Masses and widths are in MeV.

r	χ^2	M	g_1	M_{1450}	g_{1450}
1.05	2521.9	1003.7	228.7	1415.9	349.0
1.15	2501.4	1007.1	242.7	1413.7	333.0
1.25	2492.0	1011.8	264.7	1416.9	300.9
1.35	2499.7	1017.8	287.3	1418.4	279.7
1.45	2514.8	1023.8	311.5	1423.8	259.4

The amplitude squared for $a_0(980)$ is shown in Fig. 2. The peak of the curve coincides exactly with the $\overline{K}K$ threshold. Notice that the true width of the resonance is much larger than the apparent width in Fig. 2 ($\Gamma \simeq 65$ MeV) because of the threshold cusp, which pulls the $\eta\pi$ amplitude down above $s = 4m_K^2$.

D. $f_0(975)$

A critical element in the fits is $f_0(975)$. This creates a strong diagonal band in Fig. 1. But there are problems. This band lies well below the Particle Data Group (PDG) mass value, and it is considerably wider. How does this arise?

In order to understand this point it is necessary to understand $f_0(975)$. It is not a simple Breit-Wigner resonance. The fits of Zou and Bugg [11] reveal a second-sheet pole at $988 - i23$ MeV and a third-sheet pole at 797 ± 185 MeV. (The resonance full width is twice the imaginary part of these pole positions.) The second sheet pole is reached through the $\pi\pi$ cut below the $K\overline{K}$ threshold, and represents a nearly bound state of the $K\overline{K}$ channel. In $\overline{p}p$ annihilation, one has to treat carefully the cou-

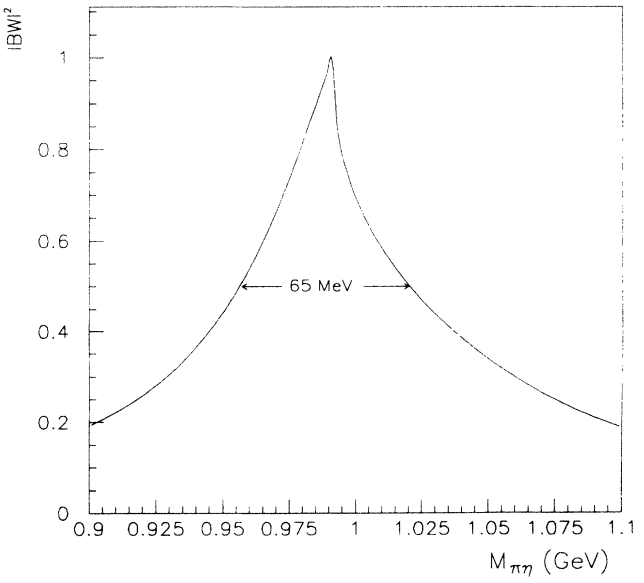

FIG. 2. $|a_0(980)|^2$ vs $M_{\eta\pi}$ in GeV.

pling to $f_0(975)$ via the intermediate $K\overline{K}$ channel. In annihilation reactions, the numerator may be different. This reflects the fact that coupling to the initial $\bar{p}p$ state is different for $\pi\pi$ and $K\overline{K}$. The numerator $N(s)$ of Eq. (19) therefore plays a critical role in fitting annihilation data.

Despite these refinements, the width of $f_0(975)$ in the $\eta\pi^0\pi^0$ data is still larger than suggested by CERN-Munich data. A free fit to the annihilation data gives a width of 108 MeV compared with the 46 MeV of Zou and Bugg. Enforcing the 46 MeV width increases χ^2 for the fit to $\eta\pi^0\pi^0$ data by 200, a highly significant amount. A combined fit weighting annihilation data equally with CERN-Munich data gives a width of 75 MeV, whether form A or form C is used and χ^2 is increased only marginally (~ 30). Fits are shown to the Cern-Munich data in Fig. 3(a). For the combined fit with form C, pole positions are $M = 983 - i37$ MeV on sheet II and $M = 996 - i103$ MeV on sheet III. These pole positions are more reliable than those of form A, since the latter has several strongly correlated parameters.

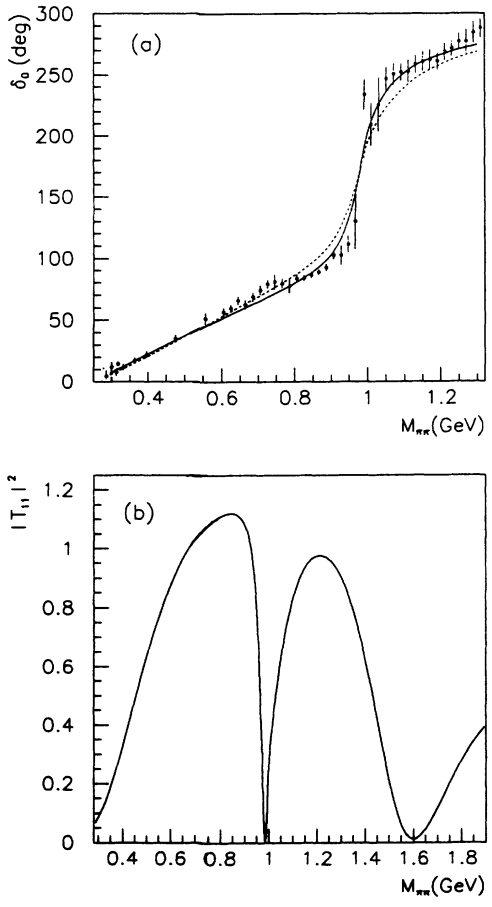

FIG. 3. (a) The phase shift δ_S (in degrees) for S-wave $\pi\pi$ elastic scattering against $M_{\pi\pi}$ (in GeV). The solid line is our fit with $\Gamma = 75$ MeV. The dashed line is a free fit to $\eta\pi^0\pi^0$ data with a width of 108 MeV. (b) The corresponding intensity vs $M_{\pi\pi}$. The vertical scale is arbitrary.

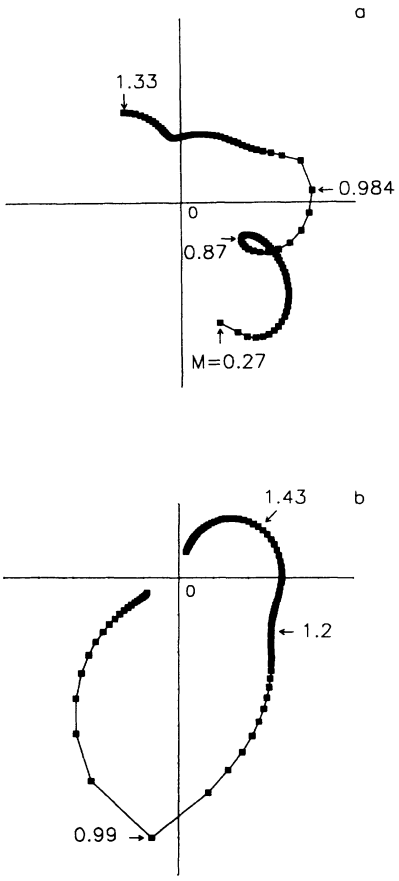

FIG. 4. (a) The $\pi\pi$ S-wave amplitude for $\bar{p}p \to \eta\pi\pi$; (b) the $\eta\pi$ S-wave amplitude. The scale is arbitrary. Points are equally spaced in s.

The Argand diagram of the $\pi\pi$ S-wave amplitude for $\bar{p}p \to \eta\pi^0\pi^0$ is shown in Fig. 4(a). There is a conspicuous signal due to $f_0(975)$ at the upper right of the diagram, and a cusp at 875 MeV due to destructive interference with the background σ amplitude.

E. $f_0(1365)$

This resonance is definitely required by the $\eta\pi^0\pi^0$ data. Removing it from the fit, χ^2 increases by 818 for 1289 points; also the convergence to the minimum deteriorates dramatically. If we fit only $\eta\pi^0\pi^0$ data and vary the mass and width of $f_0(1365)$, they optimize at $M = 1331$ MeV, $\Gamma = 307$ MeV for form A, and similar values for forms B and C. However, the χ^2 improvement compared with a combined fit including $3\pi^0$ and $\eta\eta\pi^0$ data is only 27.5. The $f_0(1365)$ resonance shows up clearly on the Argand diagram of Fig. 4(a) at the upper left of the figure.

This resonance contributes to the bottom left corner of the Dalitz plot, Fig. 1. In the same region, $f_2(1270)$ contributes, but is suppressed by the $L = 2$ centrifugal barrier for production from the initial $^1S_0$ state. We have included $f_2(1270)$ in the fits and it gives an improvement of 36 in χ^2. This is rather small, but we have retained this

amplitude in order to assess quantitatively the effect of the $L = 2$ centrifugal barrier, a point of general interest.

F. $a_0(1450)$

This is a new resonance discovered in the $\eta\pi^0\pi^0$ data and will therefore be discussed in some detail. It does not appear as a clear peak in the data but is revealed by interference effects. Consequently its parameters are rather sensitive to the way in which other amplitudes are treated. If other amplitudes are treated in the simplest possible way, with some sacrifice in χ^2, $a_0(1450)$ makes an improvement in χ^2 for $\eta\pi^0\pi^0$ data from 3009 to 2056 for 1289 data points. The mass optimizes cleanly at 1417 MeV; see Table IV. In this simplified fit, the parameters of $a_2(1320)$ are fixed at values of the Particle Data Group: $M = 1318.2$ MeV, $\Gamma = 113$ MeV. In addition $a_2'(1620)$ is omitted and form A is used for the $\pi\pi$ S wave with only three Λ parameters, Λ_1–Λ_3.

The Argand diagram for the $\eta\pi$ S wave is shown in Fig. 4(b). There is a large loop due to $a_0(980)$ with a 90° phase change at the $\overline{K}K$ threshold; at higher energies, there is a smaller loop due to $a_0(1450)$. There is a close similarity between Fig. 4(b) and the prediction of Weinstein and Isgur [16], reproduced in Fig. 5; the phase difference of about 180° between the two figures is simply a matter of the overall definition of phases.

The requirement for $a_0(1450)$ is demonstrated in Fig. 6, which displays the signs of the discrepancies on the Dalitz plot when the $a_0(1450)$ is (a) included, (b) omitted. In the latter, there are clear systematic effects over large areas of the Dalitz plot. In addition, when $a_0(1450)$ is omitted, the parameters of $a_0(980)$ are modified to values which are ridiculous: The mass of $a_0(980)$ moves to 1113 MeV and the width to 549 MeV, compared with PDG values of 976 ±6 MeV and 57±11 MeV. What is in fact happening is that the two resonances of Fig. 4(b) are being replaced by a single broad resonance midway between them. This is quite incompatible with other data sources. So $a_0(1450)$ is definitively required by the data.

When the simplifications of the amplitudes described in the first paragraph of this section are dropped by introducing $a_2'(1620)$ and freeing the parameters of $a_2(1320)$, it is possible to reduce χ^2 for $\eta\pi^0\pi^0$ data to 1603, a significant improvement. The price, however, is that the mass of $a_0(1450)$ becomes less well determined, and tends to drift to higher values. We have stepped the mass of $a_0(1425)$ by 25 MeV, reoptimizing all other parameters for each mass. Table V shows the result for the simplified fit with $\chi^2 = 2056$ for $\eta\pi^0\pi^0$ data. The mass optimizes at 1416 MeV and χ^2 rises strongly and roughly parabolically away from this mass. The same exercise has been repeated for the solution with $\chi^2 = 1603$, i.e., including $a_2'(1620)$; results are displayed in Table VI. The mass of $a_0(1450)$ increases slightly to 1436 MeV and the χ^2 minimum becomes slightly less well defined. For this fit, $\chi^2 = 1169$ for $3\pi^0$ data for 861 DF and 425 for $\eta\eta\pi^0$ data for 311 DF. For the $\pi\pi \to \pi\pi$ S-wave amplitude, it is 118 for 107 DF. Parameters of the fit are given in Table VII. Table VIII shows correlations between fitted parameters

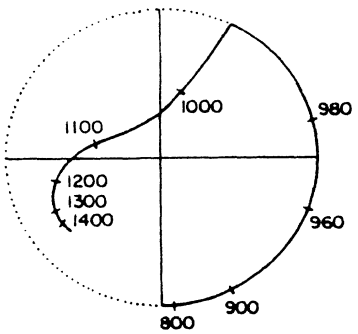

FIG. 5. The prediction of Weinstein and Isgur [16] for $\pi\eta \to \pi\eta$.

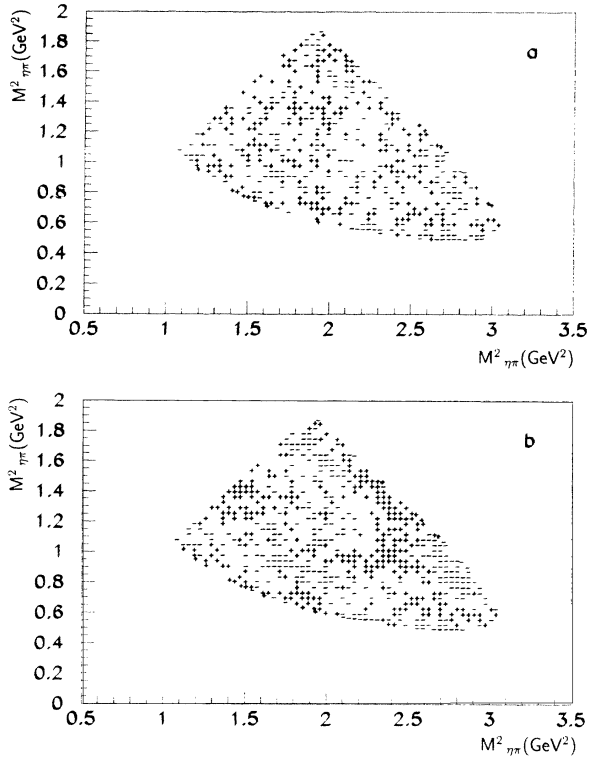

FIG. 6. Signs of discrepancies between $\eta\pi^0\pi^0$ data and the fit (a) in the best fit, (b) omitting $a_0(1450)$; + signs indicate that the fit gives a larger cross section than the data.

TABLE V. Stepping M_{1450} with $a_0(980)$ constrained as described in the text. This fit does not contain $a_2'(1620)$. Only $\eta\pi^0\pi^0$ data are fitted. Masses and widths are in MeV.

M_{1425}	$\Delta\chi^2$	g_{1450}
1366.7	36.9	368.3
1391.7	12.6	344.1
1416.7	0.0	306.3
1441.7	18.9	283.9
1466.7	30.7	306.6

TABLE VI. As in Table V, but including $a_2'(1620)$. Only $\eta\pi^0\pi^0$ data are fitted. Masses and widths are in MeV.

M_{1450}	$\Delta\chi^2$	g_{1450}
1386	33.9	353.5
1411	10.6	337.3
1436	0.0	318.5
1461	7.6	300.0
1486	41.6	295.8

when the mass of $a_0(1450)$ is moved in 25 MeV steps.

Using form C for the $\pi\pi$ S wave, the optimum χ^2 is 1620 for $\eta\pi^0\pi^0$ data and the mass of the resonance floats up to 1454 MeV. Figure 7 shows χ^2 vs the mass of $a_0(1450)$. Fitted parameters are given in Table IX. Here $\chi^2 = 401$ for $\eta\eta\pi^0$ and 1082 for $3\pi^0$ data, but using four Λ parameters for the $\pi\pi$ S wave compared with three using form A. In this fit, the $a_0(980)$ is not constrained at half-height; this accounts for the difference in mass and width of $a_0(980)$ compared with Table VII. The latter is more reliable. Despite superficial differences in formulas and coupling constants compared with form A, the Argand diagrams are very close in the two fits. This is illustrated for the S waves in Fig. 8.

From Fig. 7, it is evident that the mass of $a_0(1450)$ is not very well determined. From Tables V and VI, one sees that the mass is sensitive to assumptions about other amplitudes. A reasonable compromise, covering all fits with parametrizations A–C is $M = 1435 \pm 40$ MeV, $\Gamma = 270 \pm 40$ MeV. The errors correspond to an increase in χ^2 of 25. Likewise, a reasonable compromise between parametrizations A–C for $f_0(1365)$ and $f_0(1520)$ is $M_1 = 1340 \pm 40$ MeV, $\Gamma_1 = 255^{+60}_{-40}$ MeV and $M_2 = 1505 \pm 20$ MeV, $\Gamma_2 = 150 \pm 20$ MeV.

Earlier, the GAMS group [17] claimed to observe an a_0 resonance with $M = 1322 \pm 30$ MeV, $\Gamma = 130 \pm 30$ MeV. These values are ruled out by Crystal Barrel $\eta\pi^0\pi^0$ data. They give rise to an increase in χ^2 of 405. If only the mass is set to the GAMS value of 1322 MeV, $\Delta\chi^2 = 68$ and the width is 504 MeV.

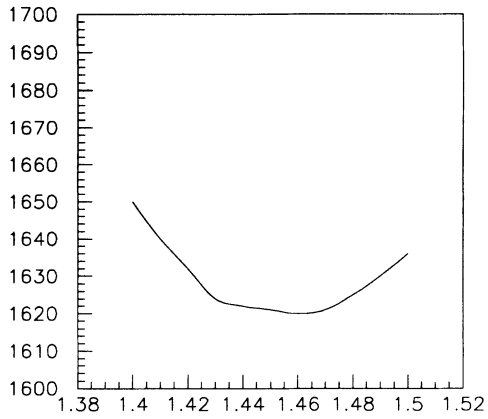

FIG. 7. χ^2 for $\eta\pi^0\pi^0$ data vs the mass of $a_0(1450)$ (GeV) using form C for the $\pi\pi$ S wave.

G. $\eta\pi$ P wave

GAMS [18] reported evidence for an exotic 1^{-+} $\eta\pi$ resonance $M(1405)$ with $\Gamma = 180 \pm 20$ MeV. It is not in Crystal Barrel $\eta\pi^0\pi^0$ data, though there is a significant nonresonant $\eta\pi$ P wave. Omitting this P wave, χ^2 increases by 596, a highly significant amount. Without it, the discrepancies between fit and data are distributed over a large part of phase space, rather than being localized. This is immediately a pointer to the fact that it is not a narrow resonance. The fit becomes worse particularly for the $a_2(1320)$ peak at the upper right edge of the Dalitz plot, feature C of Fig. 1.

Our fits use a resonance form

$$f_{1405} = \frac{\Lambda_{1405} B_1(p) B_1(q) P_1(\cos\theta)}{s - M^2 + iM\Gamma}, \tag{31}$$

where $\Gamma = gB_1^2(q)\rho_{\eta\pi}$. A free fit gives $M = 1413$ MeV, $\Gamma(M^2) = 687$ MeV. However, there is no real evidence for a resonance at all, and the form of Eq. (31) is nothing more than a convenient parametrization. Replacing this equation with a threshold factor $pq\cos\theta$ multiplied by

TABLE VII. Parameters fitted to $\bar{p}p \to \eta\pi^0\pi^0$, $3\pi^0$, and $\eta\eta\pi^0$ data using form A for the $\pi\pi$ S wave and including $a_2'(1620)$ in the fit; $a_0(980)$ is constrained at half-height as described in the text. Units are GeV.

Amplitude	M	$(\Gamma\rho)_{\rm res}$	Λ
$a_0(980)$	0.999	$g_{\eta\pi} = 0.221$ $r = 1.16$	1.0
$a_0(1450)$	1.436	0.273	$-0.661 + i0.612$
$a_2(1320)$	1.317	0.116	$-2.712 - i0.329$
$a_2'(1620)$	1.624	0.174	$0.663 - i0.336$
$\eta\pi$ P wave	1.413	0.687	$1.241 + i2.999$
$f_0(1365)$	1.365	0.267	$-5.661 - i0.622$
$f_0(1520)$	1.519	0.145	
$f_2(1270)$	1.275	0.205	$-0.159 + i0.693$
$\pi\pi$ S wave	$\Lambda_1 = -4.376 - i21.374$	$\Lambda_2 = -0.863 + i24.607$	
	$\Lambda_3 = -2.508 - i14.218$		

TABLE VIII. Stepping M_{1450} with a constraint applied to $a_0(980)$ at half-height. Both $\eta\pi^0\pi^0$ and $\eta\eta\pi^0$ data are fitted simultaneously and $a_2'(1620)$ is varied in the fit. Values of M, g_1, and r refer to $a_0(980)$. Masses and widths are in MeV. ϕ_{1450} is the phase of $a_0(1450)$ relative to $a_0(980)$ in degrees.

M_{1450}	$\Delta\chi^2$	g_{1450}	M_{980}	g_1	r	ϕ_{1450}
1375	50.8	373	999.3	211	1.12	98
1400	23.4	353	999.3	214	1.14	113
1425	5.6	326	999.4	221	1.16	130
1437.5	0.0	317	999.6	225	1.17	138
1450	3.4	308	999.8	228	1.18	147
1475	18.9	282	1001.9	247	1.25	166
1500	53.7	267	1005.5	275	1.37	185

TABLE IX. Parameters fitted to $\bar{p}p \to \eta\pi^0\pi^0$ data using form C for the $\pi\pi$ S wave and including $a_2'(1620)$ in the fit. No constraint is applied to $a_0(980)$. Units are GeV.

Amplitude	M	$(\Gamma\rho)_{\rm res}$
$a_0(980)$	1.012	$g_{\eta\pi} = 0.232$ $r = 1.51$
$a_0(1450)$	1.454	0.233
$a_2(1320)$	1.313	0.117
$a_2'(1620)$	1.573	0.095
$\eta\pi$ P wave	1.214	0.901
$f_0(1365)$	1.322	0.271
$f_0(1520)$	1.497	0.136
$f_2(1270)$	1.265	0.200

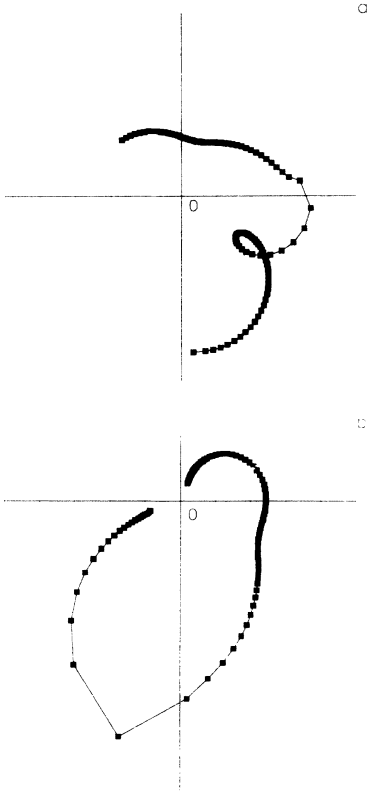

FIG. 8. Argand diagrams using form C for $\eta\pi^0\pi^0$: (a) the $\pi\pi$ S wave, (b) the $\eta\pi$ S wave. Points are equally spaced in s.

$A + Bs$ (where A and B are complex) gives a χ^2 actually superior by the small amount of 4.6.

The essential evidence for the $\eta\pi$ P wave lies, as in GAMS data, in interference with $a_2(1320)$. In the absence of interference with the $\pi\pi$ S wave and the $\eta\pi$ P wave, one expects constructive interference between the two $a_2(1320)$ bands to make the peak C at the right-hand edge of the Dalitz plot a factor of 4 larger than that at the bottom of the Dalitz plot, D. In fact, peak D is stronger than C and the bands are distorted from the vertical (and horizontal). The peak at D is at lower mass than the expected 1320 MeV and at distinctly higher mass at C. Part of the latter effect is because the intersection of the two bands is at the edge of phase space and the $P_2(\cos\theta)$ dependence plays a critical role. However, the displacement of the peak at D is a signature of P-D interference in $\eta\pi$. The situation is complicated by interference with the $\pi\pi$ S wave. Towards low $\pi\pi$ masses, point C, this amplitude is small, while near point D ($M = 1300$ MeV) it is large. Interference with the $\pi\pi$ S-wave amplitude partially accounts for the mass variation of the $a_2(1320)$ with $\cos\theta$, shown in Fig. 9.

We remark that the threshold due to $\pi f_1(1285)$, which couples to 1^{-+} with $L = 0$, occurs at 1420 MeV. However, introducing this sharp threshold into the analysis has no effect.

If GAMS parameters for $M(1405)$ are inserted into the fit, χ^2 worsens by 505, ruling out their solution.

H. $a_2'(1620)$

It is somewhat surprising that a spin-2 contribution of this mass is produced despite the $L = 2$ centrifugal barrier. However, omitting $a_2'(1620)$ makes χ^2 worse by

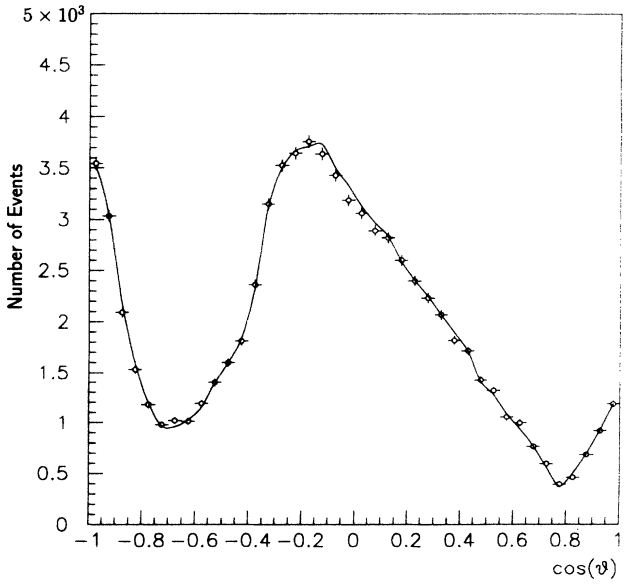

FIG. 9. The angular distribution in the $\eta\pi$ rest frame for masses between 1260 and 1500 MeV. The solid curve is the fit. The sign of θ is chosen so that $\cos\theta = +1$ near C and $\cos\theta = -1$ near D.

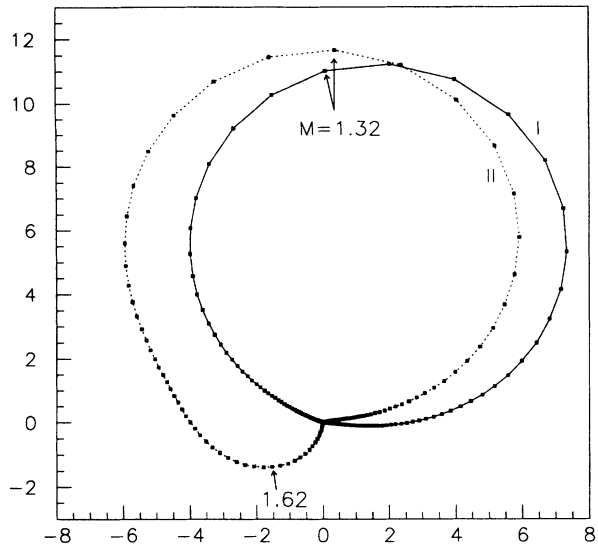

FIG. 10. The Argand diagram for the $\eta\pi$ D wave. The curve labeled I is due to $a_2(1320)$ alone, and that labeled II is due to $a_2(1320) + a_2'(1620)$. Points are equally spaced in s.

130 for form C of the $\pi\pi$ S wave and by similar amounts for the other two forms. Some of the improvement in χ^2 is actually due to changes in $f_0(975)$ rather than to the presence of $a_2'(1620)$. When it is introduced, it allows systematic changes in the $\pi\pi$ S wave near the 875 MeV cusp and an improved fit to the region labeled B on the Dalitz plot, Fig. 1. The feature E in Fig. 1 peaks at $M_{\eta\pi} = 1.67$ GeV, but is well described in all fits and seems to have no specific connection with $a_2'(1620)$.

It is possible that $a_2'(1620)$ is a Regge recurrence of $a_2(1320)$. The Argand diagram for the $\eta\pi$ D wave in this fit is shown in Fig. 10. The curve labeled I is that for $a_2(1320)$ alone, while that for $a_2(1320) + a_2'(1620)$ is shown as II. Apart from a small phase rotation between the two curves, it is evident that the data demand an enhancement of the amplitude at high mass, and a phase advance. This is reminiscent of a similar effect in the fit

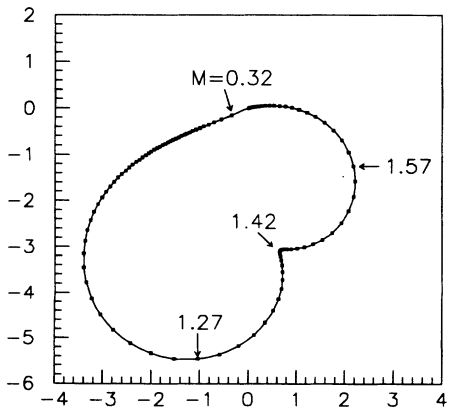

FIG. 11. The Argand diagram for the $\pi\pi$ D-wave amplitude fitted to $3\pi^0$ data.

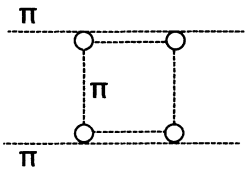

FIG. 12. The box diagram for production of two resonances.

to $3\pi^0$ data, where the D-wave Argand diagram is shown in Fig. 11. An alternative explanation of both plots is the opening of inelastic thresholds due to $I = 0$, $J^P = 2^+$ $\rho\rho$, and $I = 1$ $\rho\omega$ channels around 1550 MeV. Any threshold of this variety creates a phase advance by dispersive effects, essentially through processes of the form shown in Fig. 12. A resonance interpretation is therefore not clear-cut, unless the data demonstrate clearly the phase variation characteristic of the resonance, as is the case for $f_0(1520)$ in $3\pi^0$ data.

I. Coupling to inelastic channels

In several places we have tried including inelastic thresholds explicitly. None has any significant effect in improving the fit to $\eta\pi^0\pi^0$ data. The data of Alston-Garnjost *et al.* [19] show that the 4π cross section rises steeply from $M = 1$ to 1.6 GeV and overtakes the 2π and $\overline{K}K$ cross sections rapidly above about 1.2 GeV. The rise of the 4π cross section may be fitted approximately with a Fermi function

$$\Gamma_{4\pi} = \frac{\gamma_0}{1 + \exp(s_0 - \alpha s)}, \tag{32}$$

with $s_0 = 5.76$, $\alpha = 4$ GeV^2. (a) We have tried adding $\Gamma_{4\pi}$ to the denominator of $a_0(1450)$ and also making this the complete width. Neither change has any significant effect on the goodness of fit. (b) Likewise, we have tried substituting $\Gamma_{4\pi}$ into the denominator for M_{1405}. This does not improve the fit. (c) We have tried adding $\Gamma_{4\pi}$ to the denominator of f_{1320}, without significant improvement. (d) Finally, we have tried including Γ_{KK} in $a_2(1320)$ and $a_0(1450)$, without significant effect.

J. Branching ratios

Contributions of each amplitude squared have been summed over the Dalitz plot. Normalizing to 100% for the full amplitude squared, branching fractions are given in Table X for the fits with forms A, B, and C. For form A, it is not possible to separate accurately the individual contributions of $f_0(1365)$ because of the potential double-counting problem, and so only the total contribution from the $\pi\pi$ S wave is shown. Note that individual contributions do not add up to 100%, because of strong interferences. The total branching fraction of the $\eta\pi^0\pi^0$ channel is $(6.7 \pm 1.2) \times 10^{-3}$.

TABLE X. Branching fractions in percent, normalized to 100% for the full amplitude squared.

State	Form A	Form B	Form C
$\pi\pi$ S wave		41.0	38.5
$f_0(1365)$	39.4	7.7	6.5
$f_0(1520)$		1.8	0.5
$f_2(1270)$	0.17	0.10	0.05
$a_0(980)$	18.7	15.0	22.8
$a_0(1425)$	6.0	4.7	3.8
$\eta\pi$ P wave	10.0	5.8	6.6
$a_2(1320)$	32.4	33.0	41.5
$a_2'(1620)$	2.9	2.4	0.2
Total	109.6	111.5	120.5

III. CONCLUSIONS

A consistent solution is possible fitting data on $\bar{p}p \to 3\pi^0$, $\eta\eta\pi^0$, and $\eta\pi^0\pi^0$ at rest assuming annihilation purely from the initial $^1S_0$ state. The $\eta\pi^0\pi^0$ data reveal the presence of a new $I = 1$, $J^{PC} = 0^{++}$ resonance with a mass 1435 ± 40 MeV and $\Gamma = 270 \pm 40$ MeV. It is natural to interpret this resonance as a partner of $f_0(1365)$ and $K_0^*(1430)$ in a $\bar{q}q$ nonet.

The $\eta\pi^0\pi^0$ data also allow significant improvements in the determination of properties of $f_0(975)$ and $a_0(980)$. In particular, the ratio of branching ratios $r = g_{KK}/g_{\eta\pi}$ for $a_0(980)$ is determined to be 1.16 ± 0.18. They also require a significant but nonresonant $\eta\pi$ P wave. There is tentative evidence for activity in the $\eta\pi$ D wave above $a_2(1320)$, but it is premature to say whether this is due to inelastic thresholds or a Regge recurrence of $a_2(1320)$ or both.

ACKNOWLEDGMENTS

V.V.A. and A.V.S. are grateful to the SERC and the Royal Society for financial assistance in order to participate in the amplitude analysis. We acknowledge financial support from the U.K. Science and Engineering Research Council. We thank Dr. K. Peters, Dr. I. Augustin, and Dr. N. Winter for making available the Crystal Barrel data in numerical form. We are grateful to Dr. D. Morgan for extensive discussion about the $\pi\pi$ S wave.

[1] E. Aker *et al.*, Phys. Lett. B **260**, 249 (1991).
[2] C. Amsler *et al.*, Phys. Lett. B **291**, 347 (1992).
[3] V.V. Anisovich *et al.*, Phys. Lett. B **323**, 233 (1994).
[4] V.V. Anisovich, D.V. Bugg, A.V. Sarantsev, and B.S. Zou, Phys. Rev. D **50**, 1972 (1994).
[5] B. May *et al.*, Z. Phys. C **46**, 191 (1990); **46**, 203 (1990).
[6] C. Amsler *et al.*, Phys. Lett. B (to be published).
[7] Particle Data Group, K. Hikasa *et al.*, Phys. Rev. D **45**, S1 (1992).
[8] K. Peters, Sov. J. Nucl. Phys. **55**, 786 (1992).
[9] N. Winter, Ph.D. thesis, University of Karlsruhe, 1991.
[10] W. Flatté, Phys. Lett. **63B**, 224 (1976).
[11] B.S. Zou and D.V. Bugg, Phys. Rev. D **48**, R3948 (1993).
[12] G. Grayer *et al.*, Nucl. Phys. **B75**, 189 (1974).
[13] K.L. Au, D. Morgan, and M.R. Pennington, Phys. Rev. D **35**, 1633 (1987).
[14] C. Amsler *et al.*, Phys. Lett. B **327**, 425 (1994).
[15] W. Lockman, in *The Hadron Mass Spectrum*, Proceedings of the Conference, St. Goar, Germany, 1990, edited by E. Klempt and K. Peters [Nucl. Phys. B (Proc. Suppl.) **21**, 55 (1991)].
[16] J. Weinstein and N. Isgur, Phys. Rev. D **27**, 588 (1983).
[17] E. Boutemeur *et al.*, in *Hadron 89*, Proceedings of the International Conference on Hadron Spectroscopy, Corsica, France, edited by F. Binon, J.-M. Frère, and J.-P. Peigneux (Editions Frontières, Gif-sur-Yvette, 1989), p. 119.
[18] D. Alde *et al.*, Phys. Lett. B **205**, 397 (1988).
[19] M. Alston-Garnjost *et al.*, Phys. Lett. **36B**, 152 (1971).

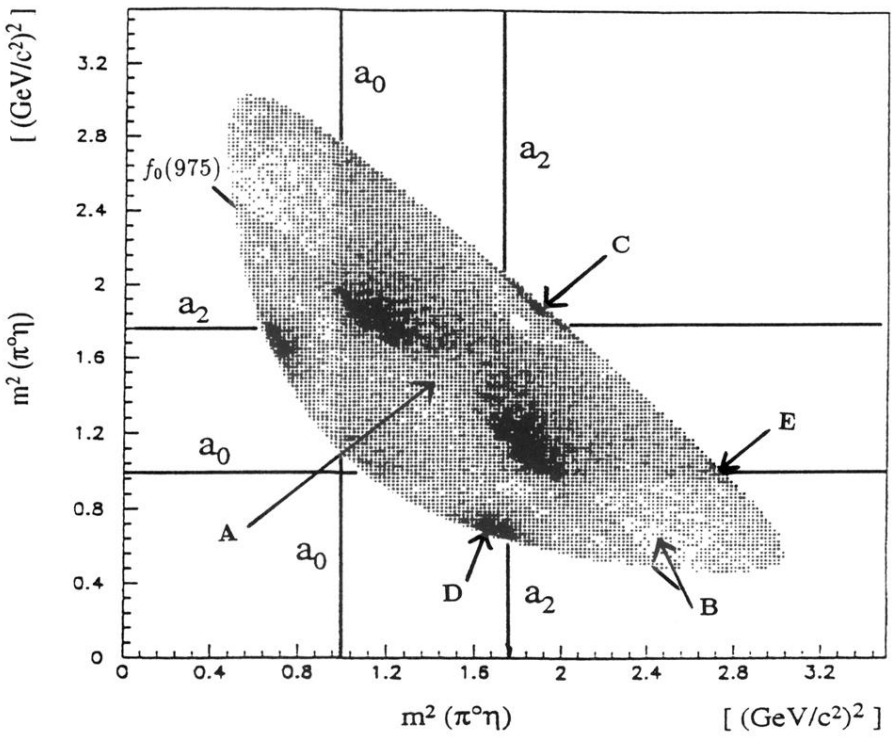

FIG. 1. The Dalitz plot for $\bar{p}p \to \eta\pi^0\pi^0$ at rest.